Surface & Coatings Technology 496 (2025) 131663

Contents lists available at ScienceDirect

Surface & Coatings Technology

journal homepage: www.elsevier.com/locate/surfcoat

Stoichiometry modulation of molybdenum oxide thin films by direct sputtering for energy applications

Salvatore La Manna [a,b,*], Giorgia Franzò [b], Antonio Terrasi [a,b], Guglielmo G. Condorelli [c], Maria Miritello [b]

[a] Dipartimento di Fisica e Astronomia "Ettore Majorana", Università di Catania, via S. Sofia 64, 95123 Catania, Italy
[b] IMM-CNR, Sede Catania (Università), via S. Sofia 64, 95123 Catania, Italy
[c] Dipartimento di Scienze Chimiche, Università di Catania, viale A. Doria 6, 95125 Catania, Italy

ARTICLE INFO

Keywords:
Oxygen vacancies
Oxide
Photovoltaics
Sub-stoichiometry
Band gap engineering

ABSTRACT

Stoichiometry of molybdenum oxide, MoO_x, thin films was controlled by simply modulating the argon working pressure during the non-reactive sputtering deposition. Rutherford Backscattering Spectrometry revealed that the O/Mo ratio increased between 2.6 and 3.0 as the argon pressure increased. X-Ray Photoemission Spectroscopy (XPS) analyses pointed out that the sub-stoichiometry led to the formation of oxygen vacancies, closely related to the presence of Mo^{5+} reduced oxidation state, while in fully stoichiometric films only Mo^{6+} oxidation state appeared. The strong correlation between composition and optical properties was demonstrated through optical absorption measurements. Sub-stoichiometric films exhibited a narrower bandgap and significant infrared absorption at 1.55 eV, attributed to increased disorder and a higher number of defects, such as oxygen vacancies. Finally, by merging the XPS and optical absorption data, we demonstrated that the band structure of MoO_x was effectively controlled by simply modulating the Argon deposition pressure. This tunability offers significant potential for tailoring the optical and electronic properties of MoO_x for applications in energy storage, photovoltaic and photonic devices.

1. Introduction

In recent years, the scientific community has dedicated significant efforts to the implementation of Transition Metal Oxides (TMOs) due to their distinctive electronic structure. Their application fields span from photovoltaics [1] to organic light emitting diodes [2], batteries [3,4], sensors [5], photocatalysis [6] and electrochemical water splitting [7,8]. Among TMOs, molybdenum oxide stands out for its environmentally friendly nature, cost-effectiveness and versatility [9]. The wide flexibility arises from the peculiar characteristics of its various oxidation states. Its fully stoichiometric form (MoO_3) is characterized by a wide bandgap (>3 eV) and insulating behavior, while its sub-stoichiometric forms, MoO_x $2 < x < 3$, have narrower bandgaps and increased conductivity, strongly ruled by the x value [10]. These features are closely related to O vacancies concentration, that make tunable the oxide electronic structure. The induced defect states within the forbidden gap depend on the reduction degree, defining the optical properties, in terms of bandgap and optical absorption [10,11]. The resulting gradual color transition, from transparent for fully stoichiometric oxide to grayish/light blue for sub-stoichiometric oxide offers promising opportunities for integration into advanced optical systems, such as displays, adjustable mirrors, and energy-saving smart windows [12]. Furthermore, the enhanced light absorption in the visible spectrum, induced by O vacancies, has been demonstrated to significantly boost the photocatalytic activity of molybdenum oxide within this critical wavelength range, as a function of sub-stoichiometry [10]. Control of oxygen deficiency in molybdenum oxides can also promote superior catalytic response compared to fully stoichiometric α-MoO_3 for hydrogen evolution reaction (HER) in water splitting [8]. The key factor is the oxygen vacancies concentration, since they are regarded as active sites for HER. They promote the favored adsorption of water molecules, acting as electron acceptors, thereby lowering the energy barrier for HER [8]. Also in photovoltaics, the precise control of film stoichiometry is critical for making MoO_x a viable hole-selective contact, as a substitute for the traditional p-doped a-Si thin film in silicon hetero-junction solar cells [1,13–15]. Indeed, the wide band gap and high work function (>6 eV) of

* Corresponding author at: Dipartimento di Fisica e Astronomia "Ettore Majorana", Università di Catania, via S. Sofia 64, 95123 Catania, Italy.
E-mail address: salvatore.lamanna@dfa.unict.it (S. La Manna).

https://doi.org/10.1016/j.surfcoat.2024.131663
Received 23 September 2024; Received in revised form 29 November 2024; Accepted 9 December 2024
Available online 16 December 2024
0257-8972/© 2024 The Author(s). Published by Elsevier B.V. This is an open access article under the CC BY license (http://creativecommons.org/licenses/by/4.0/).

stoichiometric molybdenum oxide though provide high transparency and exceptional hole selectivity, the charge carriers transport across the layer is limited by its insulating nature. The introduction of oxygen vacancies facilitates the hole transport via trap-assisted tunneling, but simultaneously induces an increasing reduction of transparency and of work function. Thus, fine tuning the oxide stoichiometry is essential to achieve the best trade-off between transparency, selectivity, and carrier transport [16,17].

Although various synthesis methods have been developed to produce stoichiometric and sub-stoichiometric molybdenum oxide thin films, the control of the oxide composition remains challenging for the realization of economic, large-scale, and reliable commercial devices with specific functionalities. While some physical vapor synthesis methods support large-scale thin film production, they still have some drawbacks. For example, evaporation demands a high thermal budget, has a low deposition rate, and does not permit stoichiometry modification [18]. Instead, reactive sputtering of a metallic target in oxygen ambient [6] permits varying oxide stoichiometry by modifying the oxygen partial pressure. However, this process suffers from low reproducibility, mainly due to unwanted poisoning of the metallic target, i.e. the metallic target oxidation due to its high reactivity with oxygen species in the sputtering plasma. This poisoning alters the target sputtering characteristics, leading to a significant reduction in the deposition rate and small changes in oxygen partial pressure, by making the process highly instable. To mitigate these challenges, sophisticated feedback tools, such as plasma emission monitoring or in-situ gas analysis, become fundamental to dynamically regulate the plasma condition and stabilize the sputtering regime [19].

In this work, we propose to modulate the stoichiometry of molybdenum oxide thin films by controlling a single deposition parameter, such as the argon working pressure, in non-reactive sputtering from a stoichiometric MoO_3 target. This method guaranteed a stable and reproducible process to achieve high-purity thin films with a fine and easy control over the film stoichiometry, besides composition and thickness. Compositional analysis, performed by Rutherford Backscattering Spectrometry (RBS), revealed a strong stoichiometry dependence on the Ar pressure. X-Ray Photoelectron Spectroscopy (XPS) was employed to identify the composition and chemical oxidation states as a function of stoichiometry. A particular focus was given on estimation of the percentage of the Mo^{5+} oxidation state, which is closely related to the O vacancies, in sub-stoichiometric films. Additionally, we investigated the correlation between film stoichiometry and optical properties through absorption measurements, focusing on the evaluation of optical bandgap and eventual intragap absorptions as a function of the film stoichiometry.

2. Experimental method

Molybdenum oxide thin films, MoO_x, with $2.6 \leq x \leq 3$, were grown with an AJA ultra-high vacuum magnetron sputtering system. The depositions were performed via radiofrequency (RF) sputtering of a 4 in. diameter stoichiometric MoO_3 target (Kurt J. Lesker, purity 99.95 %) on c-Si (100) substrates and on Corning Glass 2947. The chamber base vacuum was below 1×10^{-8} mbar. The sputtering atmosphere was pure Ar, with pressure varying between 4×10^{-3} mbar and 8×10^{-3} mbar, in steps of 1×10^{-3} mbar. The RF power applied to the target was kept constant at 200 W for all the depositions. No substrate heating was set.

The film stoichiometry was evaluated via RBS with a coaxial HVEE Cockroft-Walton Singletron accelerator, using a 2 MeV He^+ beam in random configuration, with the detector placed at an angle of 165° with respect to the incident beam.

The surface chemical composition was studied through XPS using a PHI 5000 VersaProbe II, with monochromatic Al-Kα excitation line at 1486.7 eV.

Film thicknesses were evaluated through a M2000 spectroscopic ellipsometer by J.A. Woollam, by applying a Cauchy model in the 300–1600 nm range.

Finally, the optical properties were studied by transmittance and reflectance measurements acquired by a Varian Cary 500 double beam UV–Vis-NIR spectrophotometer. The instrument allows to collect direct transmittance and specular reflectance spectra in the wavelength range 200–2500 nm. The direct transmittance measurements were normalized to a 100 % baseline obtained using an empty sample holder, while the reflectance measurements were carried out in specular geometry at 20° and normalized using a c-Si standard sample as reference.

3. Results and discussion

The deposited MoO_x thin films were listed in Table 1, with the respective Ar deposition pressure shown in column 2. All the films appeared homogeneous, with a granular structure and no evidence of voids or cracks for both the used substrates, c-Si (100) and Corning Glass 2947. As an example, a plan-view micrograph, obtained by Secondary Electron Microscopy, has been reported in Fig. S1 for P5 sample, deposited on c-Si at highest pressure (8×10^{-3} mbar).

RBS spectra were acquired for films grown on c-Si substrates, to resolve the signals associated with Mo, O and Si, necessary to reconstruct reliable elemental depth profiles. As an example, Fig. 1 reports the spectrum of the sample P5, deposited at the highest Ar pressure of 8×10^{-3} mbar.

Signals corresponding to Mo, O and Si are clearly identified, and the respective relative threshold energies are indicated; the absence of other peaks confirmed the high film purity. The profile of the observed peaks indicated a uniform chemical composition of Mo and O elements through the whole film thickness. For the analysis of O peak, the subtraction of Si background has been performed, as reported in Fig. 1. About the peaks intensity, Mo signal is about 9 times higher than the one relative to O, since it is proportional to the square of atomic number, Z ($Z_{Mo} = 42$ and $Z_O = 8$). It leads to higher sensitivity in the estimations of the Mo content. For all the deposited films, the atomic areal densities were estimated by integrating the relative signals, with the support of the XRUMP software; for the O atomic areal density, the integration of the peak was performed after the Si background subtraction and the relative error has been evaluated. The obtained values, along with corresponding uncertainties, have been shown on the left axis as a function of Ar pressure in Fig. 2. It is worth noting that the Mo values are multiplied by a factor of 3 for the sake of clarity. The dependence of both areal densities by Ar pressure is clearly evident in the whole range; their sum decreased by increasing Ar pressure. The total atomic density has been also estimated by using the film thickness measured by ellipsometry, with the support of Complete EASE software. Within an experimental error of 2 %, a constant thickness of 55 nm (± 1 nm) was estimated for all the samples, therefore a reduction in atomic density from 8.9×10^{22} at/cm^3 to 7.4×10^{22} at/cm^3 has been recorded by increasing Ar pressure.

A further careful comparison of the trends of O and Mo areal densities revealed a different behavior for the two species. In particular, while the Mo areal density decreased linearly across the whole investigated Ar pressure range; the O areal density remained constant from 4×10^{-3} mbar to 6×10^{-3} mbar, then it exhibited a linear decrease only at

Table 1
List of the deposited samples in the first column, the other columns report the deposition Ar pressure, with the O/Mo ratio, along with the uncertainties, as estimated by RBS measurements.

Sample	Ar pressure (mbar)	O/Mo ratio
P1	4×10^{-3}	2.6 ± 0.1
P2	5×10^{-3}	2.8 ± 0.1
P3	6×10^{-3}	3.0 ± 0.1
P4	7×10^{-3}	3.0 ± 0.1
P5	8×10^{-3}	3.0 ± 0.1

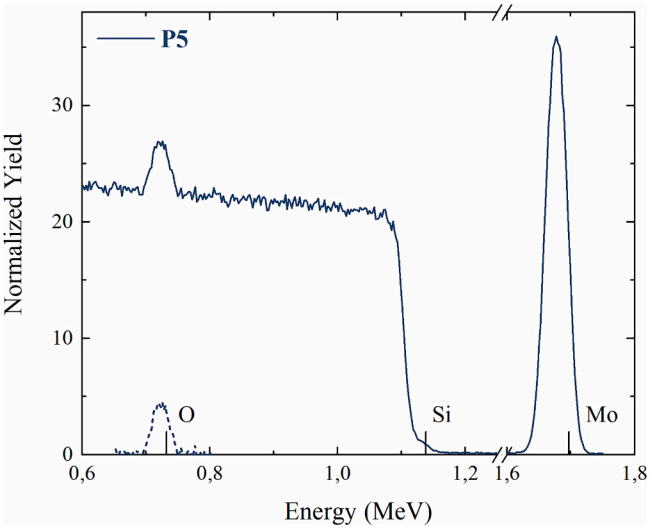

Fig. 1. RBS spectrum of P5 sample, deposited at 8 × 10^{-3} mbar. Threshold energies relative to Mo, Si and O are indicated. The O peak, after subtraction of the silicon background signal, is also depicted as dashed line.

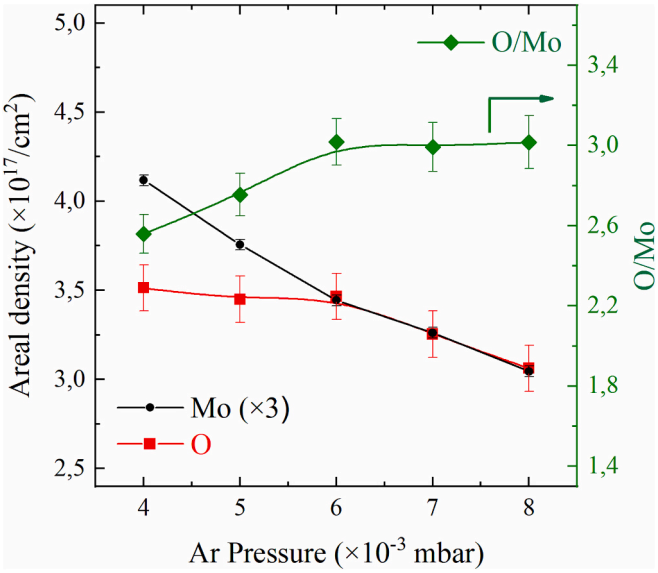

Fig. 2. Mo and O areal densities as a function of Ar pressure (left hand scale). Mo concentration values were multiplied by a factor of 3 for the sake of clarity. O/Mo ratio as a function of Ar pressure (right hand scale). The lines are guides to the eyes.

higher Ar pressures. These outcomes were attributed to the different migration behaviors of the two sputtered species within the Ar atmosphere, a phenomenon previously reported in other TMOs [20–22]. Specifically, O atoms, being six times lighter than Mo atoms, exhibited higher susceptibility to scattering at Ar pressure lower than 6 × 10^{-3} mbar. As a result, O atoms sputtered from a stoichiometric target had a lower probability of reaching the substrate compared to sputtered Mo atoms, leading to an O/Mo ratio below 3 at pressures under 6 × 10^{-3} mbar. In particular, O/Mo ratios of 2.6 ± 0.1 and 2.8 ± 0.1 were obtained for P1 and P2 samples, respectively, indicating a sub-stoichiometric composition in this pressure regime. At Ar pressure above 6 × 10^{-3} mbar, both Mo and O sputtered species underwent thermalization, with atom diffusion becoming the dominant factor in their transport. Consequently, both species were equally influenced by scattering, reaching the substrate in the same proportion as they were sputtered from the target. This resulted in an O/Mo ratio equal to 3, regardless the Ar pressure, thus replicating the target stoichiometry. The O/Mo ratio was reported on the right axis of Fig. 2 and in Columns 3 of Table 1. This fine tuning of the molybdenum oxide film stoichiometry was achieved through a highly stable and reproducible process, avoiding issues related to unwanted target poisoning [19] or the need for complex feedback control systems.

To evaluate the films quality in terms of O vacancies, which are associated with lower Mo oxidation states, XPS analyses were performed. Fig. 3(a) and Fig. 3(b) reported the Mo_{3d} core level spectra for a sub-stoichiometric film, P1, and a stoichiometric film, P5. The corresponding Gaussian– Lorentzian fitting curves, obtained after Shirley background subtraction, were achieved using standard XPS fitting software (XPS Peak 4.1). To obtain a satisfying fit, two doublets associated with the Mo^{5+} and Mo^{6+} oxidation states were required for both samples. Accounting for spin-orbit splitting, typical constraints were applied for both molybdenum oxidation states: the areas ratio of the doublet peaks, $Mo3d_{5/2}$ and $Mo3d_{3/2}$, was set to 1.5, and the spin-orbit separation was fixed to 3.15 eV. The key fitting parameters, i.e. $Mo3d_{5/2}$ peak position, Full Width at Half Maximum (FWHM), total Mo_{3d} integrated area, Lorentzian-Gaussian (L-G) percentage, and Mo^{5+} percentage, were listed in Table 2 for both Mo^{5+} and Mo^{6+} in each

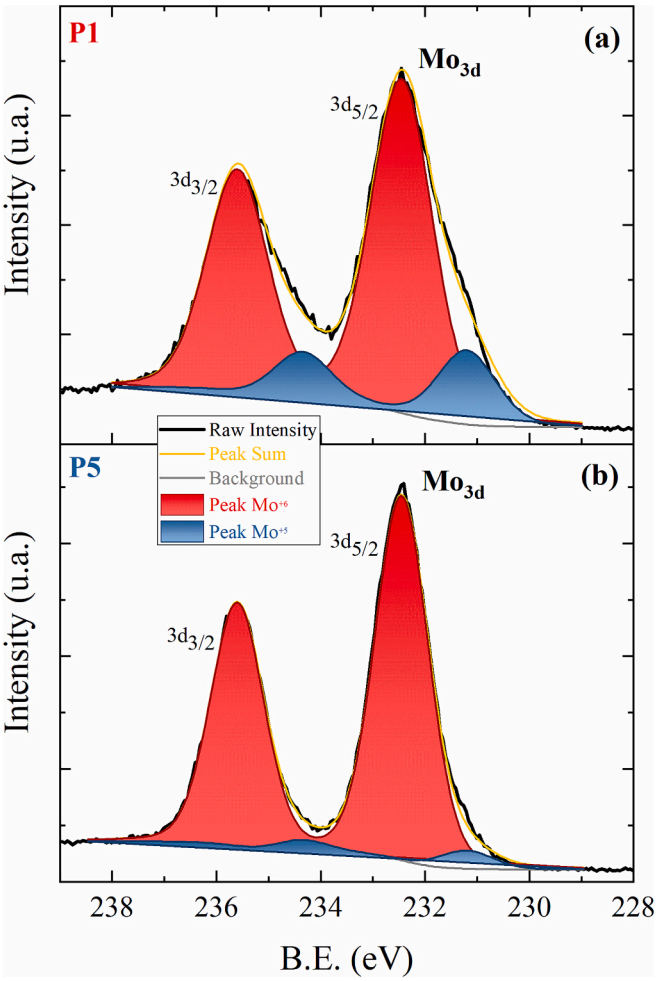

Fig. 3. XPS spectra (raw data, black line, and fitting curves, yellow line) of Mo_{3d} core levels for P1 sample deposited at 4 × 10–3 mbar (a) and P5 sample deposited at 8 × 10–3 mbar (b). The relative Shirley backgrounds and the Gaussian–Lorentzian fitting curves of Mo^{5+} and Mo^{6+} peaks, were reported for both samples. The corresponding bands were indicated. (For interpretation of the references to color in this figure legend, the reader is referred to the web version of this article.)

Table 2
Fitting parameters for Mo^{5+} and Mo^{6+} doublets of Mo_{3d} core level, for P1 and P5 samples. Peak position and FWHM of $3d_{5/2}$ peaks were reported, with the Mo_{3d} Total Integrated Area and Lorentzian-Gaussian (L-G) percentage. The estimated percentage of Mo^{5+} was also reported.

Sample	Mo^{6+}				Mo^{5+}				Mo^{5+}/Mo (%)
	$3d_{5/2}$ position (eV)	$3d_{5/2}$ FWHM (eV)	Tot. integr. area (a.u.)	L-G (%)	$3d_{5/2}$ position (eV)	$3d_{5/2}$ FWHM (eV)	Tot. integr. area (a.u.)	L-G (%)	
P1	232.45	1.40	10,728	20	231.20	1.32	2242	20	17.3
P5	232.45	1.20	12,437	14	231.20	1.20	621	14	4.8

sample. For both films, the same peak positions were observed. The $Mo^{6+}3d_{5/2}$ and $Mo^{6+}3d_{3/2}$ peaks, corresponding to the fully oxidized state, were centred at the binding energies (BE) of 232.45 eV and 235.60 eV, respectively. Meanwhile, the $Mo^{5+}3d_{5/2}$ and $Mo^{5+}3d_{3/2}$ peaks, corresponding to the lower oxidation state, were centred at BEs of 231.20 eV and 234.35 eV, respectively. These values are in good agreement with those reported in literature [6,8,23–25].

In terms of the total integrated areas of Mo^{6+} and Mo^{5+}, the fits pointed out that Mo^{6+} oxidation state was predominant in all the samples, with the Mo^{5+} contribution decreasing as Ar pressure increased. The higher Mo^{5+} percentage of 17.3 % estimated for sample P1 proved the higher concentration of oxygen vacancies, consistent with the sub-stoichiometric nature revealed by RBS measurements. Instead, the low Mo^{5+} percentage of 4.8 % for sample P5 aligned with the thermodynamic equilibrium concentration of vacancies expected at room temperature for stoichiometric films, as theoretically predicted by Mark T. Greiner et al. [26] and experimentally confirmed in Ref. [27]

The O_{1s} core levels for the P1 and P5 samples were also recorded and fitted, as shown in Fig. S2(a) and (b). The corresponding fitting parameters are detailed in Table S1. The values obtained from the fits were in good agreement with those reported in literature [28,30–32]. By integrating the total area of O_{1s}, subtracting the contribution related to surface O-impurities, and the total integrated area of Mo_{3d}, corrected with the Wagner relative sensitivity factor [33], the O/Mo ratio for both samples was calculated. Values of 2.7 and 3.0 were estimated for P1 and P5 samples, respectively, in good agreement with the results obtained through RBS analyses.

Fig. 4 reported the XPS Valence Band (VB) spectra for P1 and P5 samples. The main band, associated with the O_{2p} orbitals, ranges from about 3.00 eV below the Fermi level (positioned at 0 eV), towards higher binding energies [24,25,29,34,35]. The VB maximum was determined through linear extrapolation in the low binding energy region. The estimated value was 2.80 eV with relative to the Fermi level, independently by Ar deposition pressure, aligning with the findings of M. Ponce-Mosso et al. [6]

Another less intense signal closer to the Fermi level, centred at 1.25 eV and corresponding to Mo_{4d} orbitals, was observed for both samples, with a higher intensity in sample P1. This Mo_{4d} signal was attributed to the presence of O vacancies. It is generated when an O^{2-} ion is removed, and consequently, Mo^{6+} is reduced to Mo^{5+} to maintain the charge neutrality. As a result, the empty *4d* band becomes partially occupied with electrons, giving rise to the defect feature [24–27,34,35] at 1.25 eV: because of that, the weak band appears more evident for the sub-stoichiometric P1 sample.

To evaluate the influence of film stoichiometry and O vacancy concentration on the optical properties, the transmittance (T) and specular reflectance (R) measurements were carried out in the wavelength range 250–2500 nm for all samples deposited on Corning glass. Through transmittance and reflectance measurements, the absorption coefficient, α, was calculated using the well-known (Eq. (1)):

$$\alpha = \frac{1}{t} ln \frac{T_{sub}(1-R)}{T} \quad (1)$$

where t is the film thickness and T_{sub} is the transmittance of the Corning glass substrate. The obtained absorption coefficients are shown in Fig. 5 as a function of energy for different deposition pressures.

A decrease in the absorption coefficient was observed in samples grown at higher pressures (P3, P4, and P5) as compared to those grown at lower pressures (P1 and P2). Additionally, all samples exhibited

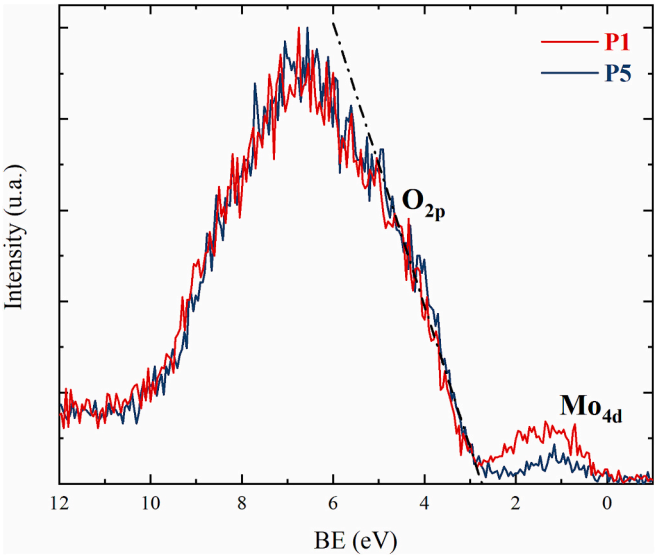

Fig. 4. XPS Valence Band spectra for P1 and P5 samples. The bands association was labelled. The dashed line represented the linear fit used to evaluate the VB maximum.

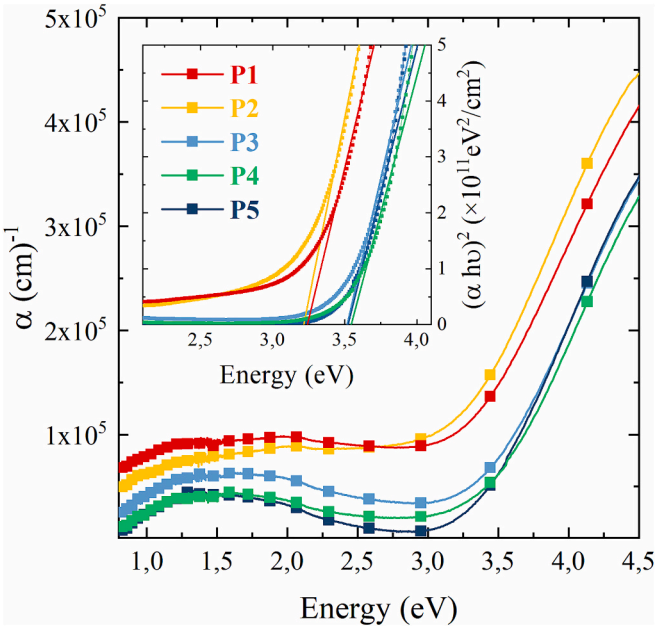

Fig. 5. Absorption coefficient of MoO_x films as a function energy for different Ar pressures. The insert showed the Tauc plots with the relative linear fits for all the samples.

higher α values at energies above 3 eV, which is attributed to band-to-band transitions [24]. Conversely, absorption tails, known as *Urbach tails*, were observed even below this threshold, likely due to the amorphous nature of the films, as demonstrated by X-ray diffraction (XRD) analyses (XRD patterns for P1 and P5 samples have been reported in Fig. S3). Their contribution was more evident for the sub-stoichiometric samples (P1 and P2) with respect to the stoichiometric ones (P3, P4 and P5). This result may be explained by the higher density of defects in the sub-stoichiometric samples, arising from a stronger structural disorder. An additional absorption contribution was observed below 2.5 eV. A broader and more intense band was recorded for the P1 and P2 samples, while a distinct peak at 1.55 eV, with a FWHM of 1.30 eV, was identified for the P3, P4, and P5 samples. This absorption contribution was strongly related to the reduced oxidation states of Mo, which were closely associated with O vacancies in the films. Specifically, the absorption peak is attributed to the charge transfer between Mo^{+5} and Mo^{+6} states, as previously reported for example in Refs [23,24]. The increased contribution of such absorption in films deposited at lower pressures (P1 and P2) indicated a higher density of O vacancies, confirming the findings from XPS measurements.

Finally, taking into account the dependence of α on photon energy, hν, when $\alpha > 10^4$ cm^{-1}, we determined the energy band gap, E_g, using the Tauc Model [36]. This method assumed that α can be expressed by the following equation (Eq. (2)):

$$\alpha = \frac{B}{h\nu}(h\nu - E_g)^{\gamma} \tag{2}$$

where B is the Tauc coefficient, and the γ factor is *1/2* or *2* for indirect or direct allowed transitions, respectively. Thus, E_g was evaluated by plotting $(\alpha \cdot h\nu)^{\gamma}$ as a function of hν. The plot was expected to exhibit a linear behavior in the high energy region, corresponding to strong absorption close to the band edge. By using $\gamma = 2$, corresponding to a direct transition, we obtained an E_g estimation by linear fit of the Tauc plots, as shown in the insert of Fig. 5. An E_g increase was observed with increasing Ar pressure, revealing values of 3.24 ± 0.05 eV and 3.22 ± 0.05 eV for the sub-stoichiometric samples, P1 and P2 respectively, and 3.52 ± 0.05 eV, 3.55 ± 0.05 eV and 3.52 ± 0.05 eV for the stoichiometric samples, P3, P4, and P5 respectively. This outcome can be explained in terms of the extended disorder and higher number of defects in the films deposited at lower pressures, P1 and P2, as reported in Refs [6,37,38]. The obtained E_g values for both sub-stoichiometric and stoichiometric samples are consistent with those reported in literature for direct allowed transition [24,39–43].

By merging the information obtained from XPS and optical measurements, we depicted the band diagrams for both sub-stoichiometric and stoichiometric molybdenum oxide films, as shown in Fig. 6(a) and (b), respectively. Specifically, the position of the VB maximum was fixed at −2.80 eV relative to the Fermi level for both stoichiometries, as determined from XPS measurements. The conduction band (CB) minima were calculated using the E_g values of 3.24 eV and 3.52 eV for the sub-stoichiometric and stoichiometric samples, placing the CB minima at +0.44 eV and +0.72 eV, respectively.

Consequently, it was worth noticing the Fermi energy is closer to the CB minimum for the sub-stoichiometric sample, giving a semiconducting n-type nature to the sub-stoichiometric films. This feature is crucial in enabling alignment of band levels with silicon, metals, oxides and organic molecules, via band bending and charge transfer doping [44].

Additionally, the band associated with oxygen vacancies was included into the diagrams. Based on absorption spectra, this band was peaked at 1.55 eV with relative to the VB maximum, positioning it at −1.25 eV below the Fermi level in both stoichiometric and sub-stoichiometric diagrams. This placement is consistent with the Mo_{4d} signal observed in the XPS spectra. For the sub-stoichiometric film, the extended band tails, revealed by optical measurements, were also included. These tails reflect a higher density of defects, making the sub-stoichiometric film more effective at absorbing light in the UV and visible ranges. This feature is strategic for enhancing photocatalytic activity, as demonstrated in Ref. [10]. Furthermore, the increased defect density improves the film electrical conductivity, facilitating better electron transfer for catalytic applications.

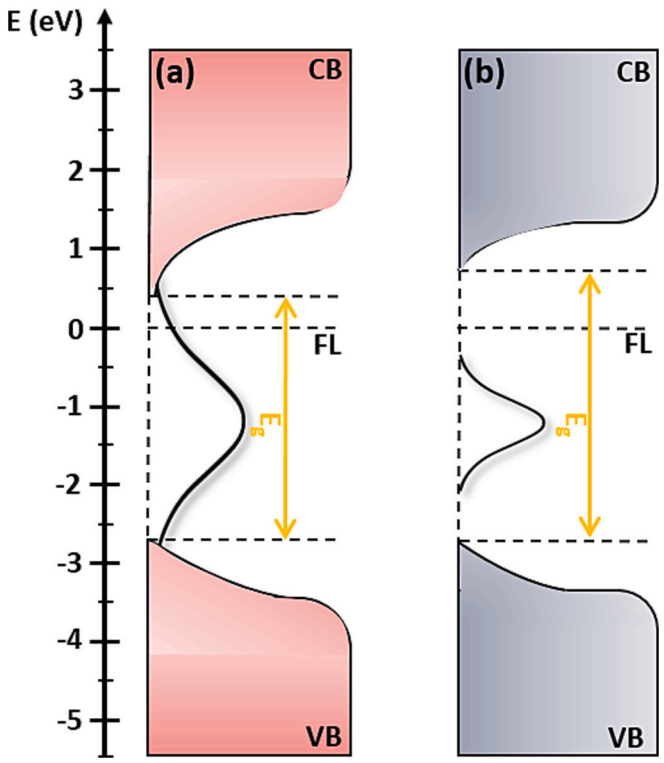

Fig. 6. Band diagrams of sub-stoichiometric (a) and stoichiometric (b) films.

4. Conclusions

In conclusion, we successfully achieved fine control over the compositional properties of high-purity molybdenum oxide thin films through the modulation of Ar pressure in non-reactive sputtering process. Films composition was estimated increasing from 2.6 to 3.0, by increasing Ar pressure, and concentration of Mo^{5+} oxidation states, correlated to the oxygen vacancy, decreasing from 17.3 % to 4.8 %. Optical measurements revealed that sub-stoichiometric films, $x < 3$, exhibited a narrower bandgap, from 3.24 ± 0.05 eV for sub-stoichiometric samples to 3.52 ± 0.05 eV for stoichiometric samples. Moreover, in sub-stoichiometric samples it was revealed a stronger infrared optical absorption, centered at 1.55 eV, originated from the higher density of oxygen vacancies and increased disorder, while stoichiometric films demonstrated reduced defect-related absorption. These findings illustrate that only one deposition parameter, Ar sputtering pressure, directly influences oxidation states and defects density in the molybdenum oxide films, by offering effective engineering of the electronic band with a fine tunability of material properties.

This study highlighted non-reactive sputtering as a straightforward, reproducible and scalable method for producing high-quality amorphous molybdenum oxide films with tailored compositions and optoelectronic properties. The demonstrated fine tuning paves the way for advances in large-area displays, photocatalysis, water splitting, photovoltaics, and photonic devices.

The following files are available free of charge. Morphology characterization by SEM, XPS spectrum of O_{1s} core level and X-ray Diffraction characterization (PDF). Supplementary data to this article can be found online at https://doi.org/10.1016/j.surfcoat.2024.131663.

CRediT authorship contribution statement

Salvatore La Manna: Writing – original draft, Investigation. **Giorgia Franzò:** Writing – review & editing. **Antonio Terrasi:** Writing – review & editing, Supervision. **Guglielmo G. Condorelli:** Writing – review & editing. **Maria Miritello:** Writing – review & editing, Supervision.

Declaration of competing interest

The authors declare that they have no known competing financial interests or personal relationships that could have appeared to influence the work reported in this paper.

Acknowledgements

The research was funded by the Italian Project PNNR "Sicilian MicronanoTech Research and Innovation Center" (SAMOTHRACE), Ecosistema dell'Innovazione, grant number ECS00000022, CUP B63C22000620005. A. Terrasi aknowledges the financial support of the project GOPV (Materiali di nuova GeneraziOne Per celle fotoVoltaiche tandem), financed by MASE (formerly MITE) - System Research Call - CSEA - TYPE A, of the Ministry of Ecological Transition. The authors thank the Bionanotech Research and Innovation Tower (BRIT) laboratory of University of Catania (Grant no. PONa3_00136 financed by the Italian Ministry for Education, University and Research, MIUR) for the XPS and XRD facilities.

The authors also acknowledge Dr. Vincenzina Strano for SEM characterization, Prof. Graziella Malandrino for XRD characterization, and C. Percolla, S. Tatì and G. Pantè for their technical support.

Data availability

Data will be made available on request.

References

[1] Luis G. Gerling, Somnath Mahato, Anna Morales-Vilches, Gerard Masmitja, Pablo Ortega, Cristobal Voz, Ramon Alcubilla, Joaquim Puigdollers, Transition metal oxides as hole-selective contacts in silicon heterojunctions solar cells, Sol. Energy Mater. Sol. Cells 145 (2016) 109–115.

[2] V. Vasanthi, N. Sivanantham, L. Saathvika, N. Gopalakrishnan, Metal oxide charge transport materials for light emitting diodes - an overview, Mater. Sci. Semicond. Process. 165 (2023) 107679.

[3] Kaiyuan Wei, Yu Jinxu Qiu, Shiping Ma Zhao, Yicheng Wei, Hongliang Li, Chao Zeng, Yanhua Cui, Tunable oxygen vacancies in MoO_3 lattice with improved electrochemical performance for Li-ion battery thin film cathode, Ceram. Int. 49 (2023) 21729–21736.

[4] Qiongyao Song, Shuhao Zhou, Shouyue Wang, Sheng Li, Xu Li, Jingxia Qiu, Insights into the oxygen vacancies in transition metal oxides for aqueous zinc-ion batteries, Chem. Eng. J. 461 (2023).

[5] H.M. Alia, E.Kh. Shokr, Y.A. Taya, Sh.A. Elkot, M.F. Hasaneen, W.S. Mohamed, Amorphous molybdenum trioxide thin films for gas sensing applications, Sens. Actuators, A 335 (2022) 113355.

[6] M. Ponce-Mosso, M. Pérez-González, P.E. García-Tinoco, H. Crotte-Ledesma, M. Morales-Luna, S.A. Tomás, Enhanced photocatalytic activity of amorphous MoO3 thin films deposited by rf reactive magnetron sputtering, Catal. Today 349 (2020) 150–158.

[7] Silvia Scalese, Fiorella Tringali, Andrea Lo Mastro, Salvatore La Manna, Giacometta Mineo, Andrea Russo, Mario Scuderi, Maria Miritello, Giorgia Franzò, Salvatore Mirabella, Antonio Terrasi, Thermally evaporated MoO_3 nanowires as oxygen evolution reaction catalysts for water splitting applications, ACS Appl. Nano Mater. 6 (2023) 22947–22955.

[8] Zhu Luo, Ran Miao, Tran Doan Huan, Islam M. Mosa, Altug S. Poyraz, Wei Zhong, Jacqueline E. Cloud, David A. Kriz, Srinivas Thanneeru, Junkai He, Yashan Zhang, Rampi Ramprasad, Steven L. Suib, Mesoporous MoO_{3-x} material as an efficient electrocatalyst for hydrogen evolution reactions, Adv. Energy Mater. 6 (2016) 1600528.

[9] Mário Gomes da Silva Júnior, Luis Carlos Costa Arzuza, Herbet Bezerra Sales, Rosiane Maria da Costa Farias, Gelmires de Araújo Neves, Hélio de Lucena Lira, Romualdo Rodrigues Menezes, A brief review of MoO_3 and MoO_3-based materials and recent technological applications in gas sensors, lithium-ion batteries, adsorption, and photocatalysis, Materials 16 (2023) 7657.

[10] Isabela Alves, Robi de Castro, Shankar Datta, Ou Jian Zhen, Andres Castellanos-Gomez, Sharath Sriram, Torben Daeneke, Kourosh Kalantar-zadeh, Molybdenum oxides – from fundamentals to functionality, Adv. Mater. 29 (2017) 1701619.

[11] Tao He, Jiannian Yao, Photochromism of molybdenum oxide, J. Photochem. Photobiol. C 4 (2003) 125–143.

[12] Natasha A. Chernova, Megan Roppolo, Anne C. Dillon, M. Stanley Whittingham, Layered vanadium and molybdenum oxides: batteries and electrochromics, J. Mater. Chem. 19 (2009) 2526–2552.

[13] Jingnan Tong, Yimao Wan, Jie Cui, Sean Lim, Ning Song, Alison Lennon, Solution-processed molybdenum oxide for hole-selective contacts on crystalline silicon solar cells, Appl. Surf. Sci. 423 (2017) 139–146.

[14] Julie Dréon, Quentin Jeangros, Jean Cattin, Jan Haschke, Luca Antognini, Christophe Ballif, Mathieu Boccard, 23.5%-efficient silicon heterojunction silicon solar cell using molybdenum oxide as hole-selective contact, Nano Energy 70 (2020) 104495.

[15] Kumar Mallem, Yong Jun Kim, Shahzada Qamar Hussain, Subhajit Dutta, Anh Huy Tuan Le, Ju Minkyu, Jinjoo Park, Young Hyun Cho, Youngkuk Kim, Eun-Chel Cho, Junsin Yi, Molybdenum oxide: a superior hole extraction layer for replacing p-type hydrogenated amorphous silicon with high efficiency heterojunction Si solar cells, Mater. Res. Bull. 110 (2019) 90–96.

[16] Shahzada Qamar Hussain, Kumar Mallem, Yong Jun Kim, Anh Huy Tuan Le, Muhammad Quddamah Khokhar, Sehyeon Kim, Subhajit Dutta, Simpy Sanyal, Youngkuk Kim, Jinjoo Park, Youngseok Lee, Young Hyun Cho, Eun Chel Cho, Junsin Yi, Ambient annealing influence on surface passivation and stoichiometric analysis of molybdenum oxide layer for carrier selective contact solar cells, Mater. Sci. Semicond. Process. 91 (2019) 267–274.

[17] Yeonjin Yi, Pyung Eun Jeon, Hyunbok Lee, Kyul Han, Hyun Sung Kim, Kwangho Jeong, Sang Wan Cho, The interface state assisted charge transport at the MoO_3/metal interface, J. Chem. Phys. 130 (2009) 094704.

[18] Jingnan Tong, Tien T. Le, Md. Wensheng Liang, Anower Hossain, Keith R. McIntosh, Parvathala Narangari, Stephane Armand, Teng C. Kho, Kean T. Khoo, Yahya Zakaria, Amir A. Abdallah, Sachin Surve, Marco Ernst, Bram Hoex, Kean Chern Fong, Impact of pregrown SiO_x on the carrier selectivity and thermal stability of molybdenum-oxide-passivated contact for Si solar cells, ACS Appl. Mater. Interfaces 13 (2021) 36426–36435.

[19] W.D. Westwood, Sputter deposition processes, MRS Bull. 13 (1988) 46–51.

[20] Wenkai Zhao, Yue Zhao, Ye Yang, Jia Li, Pinjun Lan, Jinhua Huang, Weijie Song, Direct regulation of O/W stoichiometric ratio and microstructure in tungsten oxide electrochromic films by Ar pressure using oxide target sputtering, Phys. Status Solidi A 217 (2020) 1900999.

[21] M. Acosta, D. González, I. Riech, Optical properties of tungsten oxide thin films by non-reactive sputtering, Thin Solid Films 517 (2009) 5442–5445.

[22] Jörg Neidhardt, Stanislav Mráz, Jochen M. Schneider, Erik Strub, Wolfgang Bohne, Bartosz Liedke, Wolfhard Möller, Christian Mitterer, Experiment and simulation of the compositional evolution of Ti–B thin films deposited by sputtering of a compound target, J. Appl. Phys. 104 (2008) 063304.

[23] M. Morales-Luna, S.A. Tomas, M.A. Arvizu, M. Perez-Gonzalez, E. Campos-Gonzalez, The evolution of the Mo^{5+} oxidation state in the thermochromic effect of MoO_3 thin films deposited by rf magnetron sputtering, J. Alloys Compd. 722 (2017) 938–945.

[24] Tarsame S. Sian, G.B. Reddy, Optical, structural and photoelectron spectroscopic studies on amorphous and crystalline molybdenum oxide thin films, Sol. Energy Mater. Sol. Cells 82 (2004) 375–386.

[25] Ah. Xiaxia Liao, Reum Jeong, Regan G. Wilks, Sven Wiesner, Marin Rusu, Roberto Félix, Ting Xiao, Claudia Hartmann, Marcus Bär, Tunability of MoO_3 thin-film properties due to annealing in situ monitored by hard X-ray photoemission, ACS Omega 4 (2019) 10985–10990.

[26] Mark T. Greiner, Lily Chai, Michael G. Helander, Wing-Man Tang, Lu. Zheng-Hong, Transition metal oxide work functions: the influence of cation oxidation state and oxygen vacancies, Adv. Funct. Mater. 22 (2012) 4557–4568.

[27] Katherine Inzani, Mohammadreza Nematollahi, Sverre M. Selbach, Tor Grande, Fride Vullum-Bruer, Progression of reduction of MoO3 observed in powders and solution-processed films, Thin Solid Films 626 (2017) 94–103.

[28] Shahzada Qamar Hussain, Kumar Mallem, Yong Jun Kim, Anh Huy Tuan Le, Muhammad Quddamah Khokhar, Sehyeon Kim, Subhajit Dutta, Simpy Sanyal, Youngkuk Kim, Jinjoo Park, Youngseok Lee, Young Hyun Cho, Eun Chel Cho, Junsin Yi, Ambient annealing influence on surface passivation and stoichiometric analysis of molybdenum oxide layer for carrier selective contact solar cells, Mater. Sci. Semicond. Process. 91 (2019) 267–274.

[29] Bao Yue Zhang, Ali Zavabeti, Adam F. Chrimes, Farjana Haque, Luke A. O'Dell, Hareem Khan, Nitu Syed, Robi Datta, Yichao Wang, Anthony S.R. Chesman, Torben Daeneke, Kourosh Kalantar-zadeh, Ou. Jian Zhen, Degenerately hydrogen doped molybdenum oxide nanodisks for ultrasensitive plasmonic biosensing, Adv. Funct. Mater. 28 (2018) 1706006.

[30] A.A. Mane, A.V. Moholkar, Orthorhombic MoO_3 nanobelts based NO_2 gas sensor, Appl. Surf. Sci. 405 (2017) 427–440.

[31] M. Sendova-Vassileva, Hr Dikov, P. Vitanov, G. Popkirov, R. Gergova, G. Grancharov, V. Gancheva, Magnetron sputtered molybdenum oxide for application in polymers solar cells, J. Phys. Conf. Ser. 764 (2016) 012022.

[32] Luis G. Gerling, Cristobal Voz, Ramón Alcubilla, Joaquim Puigdollers, Origin of passivation in hole-selective transition metal oxides for crystalline silicon heterojunction solar cells, J. Mater. Res. 32 (2) (2017) 260–268.

[33] C.D. Wagner, L.E. Davis, M.V. Zeller, J.A. Taylor, R.H. Raymond, L.H. Gale, Empirical atomic sensitivity factors for quantitative analysis by electron spectroscopy for chemical analysis, Surf. Interface Anal. 3 (1981) 211–225.

[34] Aitana Tarazaga Mart'ın-Luengo, Harald Köstenbauer, Jörg Winkler, Alberta Bonanni. Processing and charge state engineering of MoO_x. AIP Adv. 7 (2017) 015034.

[35] F. Werfel, E. Minni, Photoemission study of the electronic structure of Mo and MO oxides, J. Phys. C Solid State Phys. 16 (1983) 6091–6100.
[36] J. Tauc, A. Menth, States in the gap, J. Non-Cryst. Solids 8-10 (1972) 569–585.
[37] Bita Ghasemi, Fatemeh Hajakbari, Alireza Hojabri, Structural and optical properties of nanocrystalline MoO_3 thin films grown by thermal oxidation of sputtered molybdenum films, Inorg. Nano-Met. 50 (2020) 414–422.
[38] Shih-Yuan Lin, Ying-Chung Chen, Chih-Ming Wang, Po-Tsung Hsieh, Shun-Chou Shih, Post-annealing effect upon optical properties of electron beam evaporated molybdenum oxide thin films, Appl. Surf. Sci. 255 (2009) 3868–3874.
[39] A. Boukhachema, C. Bouzidi, R. Boughalmi, R. Ouerteni, M. Kahlaoui, B. Ouni, H. Elhouichet, M. Amlouk, Physical investigations on MoO_3 sprayed thin film for selective sensitivity applications, Ceram. Int. 40 (2014) 13427–13435.
[40] A. Bouzidi, N. Benramdane, H. Tabet-Derraz, C. Mathieu, B. Khelifa, R. Desfeux, Effect of substrate temperature on the structural and optical properties of MoO_3 thin films prepared by spray pyrolysis technique, Mater. Sci. Eng. B 97 (2003) 5–8.
[41] Haris Mehmood, Gence Bektaş, İlker Yıldız, Tauseef Tauqeer, Hisham Nasser, Raşit Turan, Electrical, optical and surface characterization of reactive RF magnetron sputtered molybdenum oxide films for solar cell applications, Mater. Sci. Semicond. Process. 101 (2019) 46–56.
[42] V. Nirupama, P. Sreedhara Reddy, O.M. Hussain, S. Uthanna, Structural and optical characterization of DC magnetron sputtered molybdenum oxide films, Ionics 13 (2007) 451–454.
[43] P. Adal Arasu, R. Victor Williams, The dielectric studies on sol–gel routed molybdenum oxide thin film, J. Adv. Dielect. 7 (2017) 1750011.
[44] Mark T. Greiner, Michael G. Helander, Wing-Man Tang, Zhi-Bin Wang, Jacky Qiu, Zheng-Hong Lu, Universal energy-level alignment of molecules on metal oxides, Nat. Mater. 11 (2012) 76–81.